NANO LETTERS

2009
Vol. 9, No. 4
1356-1361

Electrical and Thermal Coupling to a Single-Wall Carbon Nanotube Device Using an Electrothermal Nanoprobe

Jungchul Lee,[†,⊥] Albert Liao,[‡,⊥] Eric Pop,[‡,⊥] and William P. King*[,†,⊥]

Department of Mechanical Science and Engineering, Department of Electrical and Computer Engineering, Micro and Nanotechnology Laboratory, University of Illinois at Urbana−Champaign, Urbana, Illinois 61801

Received October 5, 2008; Revised Manuscript Received January 7, 2009

ABSTRACT

We utilize a multifunctional atomic force microscope (AFM) cantilever applying highly localized temperature and electric fields to interrogate transport in single-wall carbon nanotube field-effect transistors (CNTFETs). The probe can be operated either in contact with the CNT, in intermittent contact, or as a Kelvin probe, and can independently control the electric field, mechanical force, and temperature applied to the CNT. We modulate current flow in the CNT with tip-applied electric field, and find this field-effect depends upon both cantilever heating and CNT self-heating. CNT transport is also investigated with AFM tip temperature up to 1170 °C. Tip-CNT thermal resistance is estimated at 1.6 $\times$ 10^7 K/W and decreases with increasing temperature. Threshold force (<100 nN) for reliable contact mode imaging is extracted and used to determine set points for nanotube manipulation, such as displacement or cutting. The ability to measure thermal coupling to a single-molecule electronic device could offer new insights into nanoelectronic devices.

Devices based on carbon nanotubes (CNTs) are of significant interest due to their extraordinary electrical,[1,2] mechanical,[3] and thermal[4] properties. In general, device behavior and properties in these three physical domains are coupled. For example, the conductance of a single-wall CNT suspended over a trench was modulated by 2 orders of magnitudes when the CNT was deflected with an atomic force microscope (AFM) tip.[5] In another example, the band structure of a suspended CNT has been significantly modified by mechanical strain applied with an AFM cantilever.[6] A deep understanding of CNT device behavior requires concurrent investigation of electrical, mechanical, and thermal properties.

Scanning gate microscopy (SGM)[7] measures the current flow in a device under test (DUT) while scanning a conductive AFM tip over a sample in noncontact mode. The conductive tip acts as a moving gate electrode that locally modifies the energy levels of the device and thus affects carrier transport. Similar to other scanning probe microscopy relying on capacitance coupling, typical SGM employs dual scans along the fast scan axis where the first scan acquires surface topography in amplitude modulation (AM) mode and the second scan measures current (conductance) modulation of the DC biased DUT in lift mode to minimize topographic artifacts. SGM has been used to investigate many nanoelectronic devices including CNTs,[8,9] nanowires,[10,11] quantum dots,[12] quantum rings,[13] and, quantum point contacts.[14,15]

SGM is an ideal tool to investigate carrier transport while the CNT device is subject to local electric fields, temperature, and mechanical stress. However, no published work has reported local temperature effects during SGM mainly (due to the lack of AFM probe) capable of local heating over a wide temperature range. One recent study on laser-induced local heating of individual CNTs showed electrical conductance linearly decreases with the local temperature.[16] However the configuration prevented simultaneous AFM imaging and electrical current mapping. An AFM cantilever with an integrated heater is well suited for characterizing CNT devices where the cantilever itself is a local heat source during SGM.

In this letter, we use an electrothermal AFM cantilever capable of applying SGM experimental conditions on carbon nanotube field-effect transistors (CNTFETs). The cantilever has two parallel legs which are selectively doped to define a resistive area only near the cantilever free end.[17] Thus, it can be used as a highly localized heater and applied in nanoscale thermal manufacturing[18,19] and materials analysis.[20,21] Since the whole cantilever is doped and electrically conductive, the cantilever can apply a local electric field when the legs are biased together. Recently, we have used this cantilever to measure contact potential between the

* To whom correspondence should be addressed. E-mail: wpk@illinois.edu.
† Department of Mechanical Science and Engineering.
‡ Department of Electrical and Computer Engineering.
⊥ Micro and Nanotechnology Laboratory.

10.1021/nl803024p CCC: $40.75
Published on Web 02/26/2009

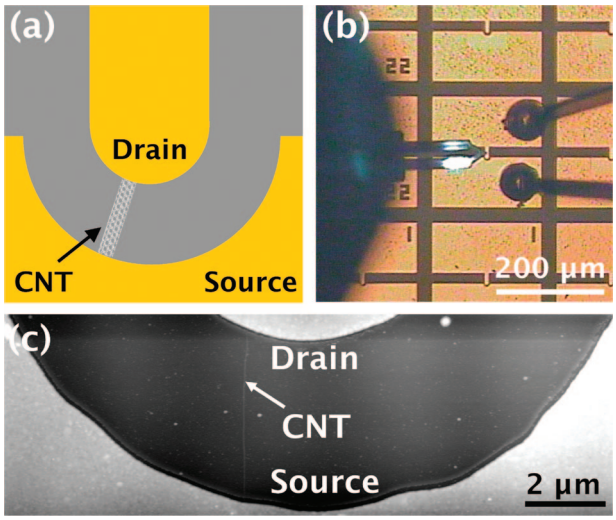

Figure 1. (a) Top view schematic of the carbon nanotube field-effect transistor (CNTFET). (b) Optical image showing the functional microcantilever probe positioned over a wirebonded CNTFET device. (c) AFM topographic image of the CNTFET with a single-wall nanotube of diameter $d \approx 2$ nm and length $L \approx 4$ μm set by the metal electrode spacing.

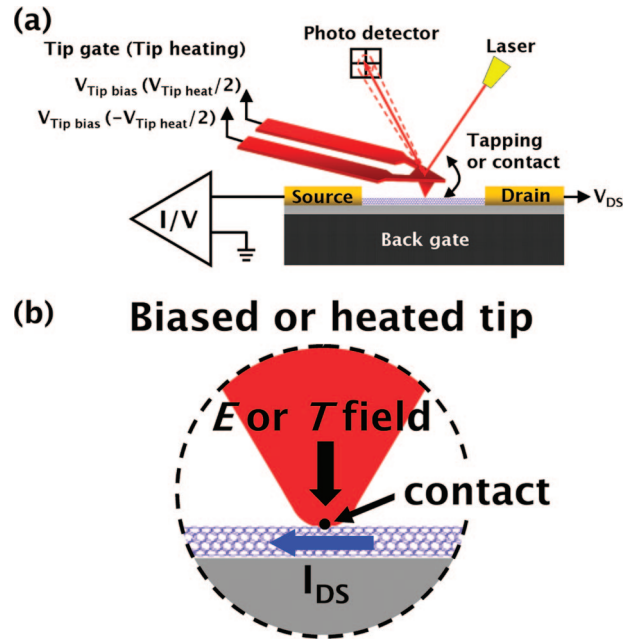

Figure 2. (a) Schematic of the experimental setup. The cantilever and CNTFET are mounted on an MFP-3D AFM, and current modulation (ΔI_{DS}) in the CNT is measured with a current-to-voltage converter in either contact or AM modes while the cantilever tip is biased or heated. (b) Zoom-in view near the apex of the cantilever tip. Mechanical stress (by continuous or intermittent contact), electric, and temperature fields can be exerted on the CNT in a highly localized fashion using a single microcantilever.

silicon tip and a gold film from room temperature to 200 °C.[22] Another advantage of this AFM cantilever is an intermediate stiffness enabling both contact and AM mode imaging. Here, we investigate current modulation in CNTFETs subject to localized temperature and electric fields in either contact or AM mode. In contrast to conventional SGM relying on an interleaved scan, current modulation in CNT devices was measured simultaneously with the topography scan such that local contact effects can be examined.

Single-wall carbon nanotubes were grown by chemical vapor deposition (CVD) from Fe catalyst on degenerately doped p+ silicon with 100 nm of thermal oxide, shown in Figure 1a.[23] After growth, electrodes were made by evaporation and lift-off patterning of 40 nm Pd over the CNTs. Concentric semicircular electrodes were used, offering better control of nanotube device length. This CNT device is a back-gated p-type FET operating at room temperature in air. To test it under AFM, each electrode was wire-bonded to a chip carrier and the device was mounted on the MFP-3D AFM (Asylum Research). Figure 1b shows an optical image of the multifunctional AFM probe and the CNTFET. The white area around the cantilever free end is the AFM laser. Figure 1c shows AFM topography of a CNTFET taken in AM mode having one semiconducting single-wall CNT between source and drain. In cases where there were more than one CNT present between electrodes, we were able to break the additional CNTs,[24,25] as outlined in the Supporting Information.

Figure 2a shows the experimental setup. The "U"-shaped cantilever made of selectively doped silicon has two parallel legs that are connected to independent metal pads. When both metal pads are tied together and biased, local electric field can be generated around the tip. When a potential difference exists between the two metal pads, the cantilever is Joule-heated and a local temperature field can be applied from the tip. For local heating, each leg is symmetrically biased with the opposite sign to maintain 0 V at the tip. This is a key step, as otherwise the electric field generated by the tip with a nonzero potential would shadow local heating effects. The cantilever was positioned over a CNTFET connected to a current-to-voltage converter to measure current modulation while the FET was subject to local electric, temperature, or stress fields. Figure 2b shows a cartoon of the cantilever tip near the apex. Mechanical stress (by continuous or intermittent contact), electric, and temperature field can be exerted on the CNT in a highly localized fashion using a single tip. The cantilever has a fundamental resonance frequency of 73.57 kHz and spring constant of 1.56 N/m. The tip radius and height for this particular cantilever are 30 and 900 nm, respectively. For contact mode operations, the contact force was <12 nN. When the contact force was >100 nN, CNTs were pushed around during imaging and eventually broken. This force level becomes a threshold for reliable contact mode imaging and determines set points for nanotube manipulation, as addressed in the Supporting Information. For AM mode operation, the free vibration and set-point amplitude were set to 337 and 55.7 nm, respectively. Since our cantilever is much softer than any commercial cantilever for dynamic AFM, AM mode imaging should be operated in a repulsive regime with a set-point amplitude below 20% of the free vibration amplitude. For both imaging modes, the scan rate and corresponding scan speed were 1 Hz and 50.08 μm/s with a scan area of 20×5 μm^2, respectively.

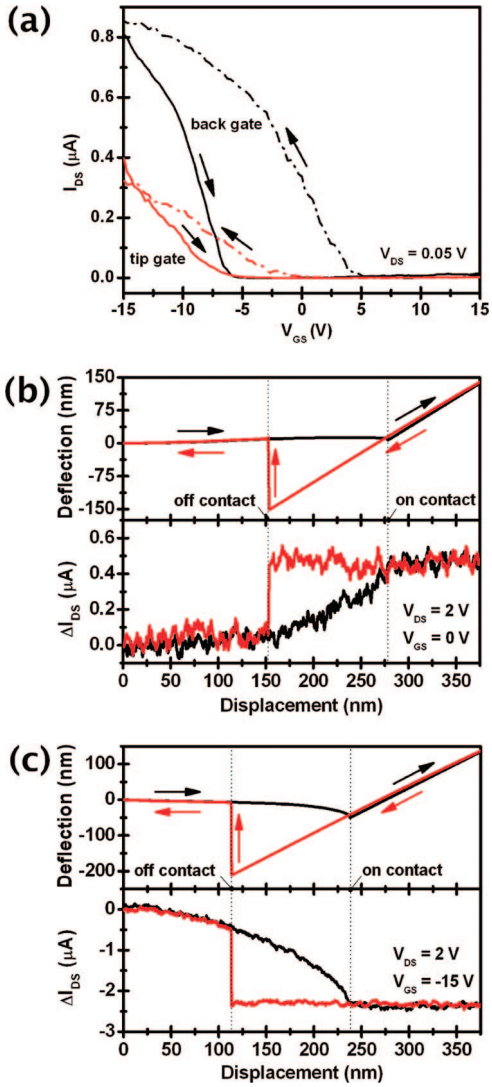

Figure 3. (a) $I_{DS}-V_{GS}$ curves for the tested device using either back gate or tip gate at $V_{DS} = 0.05$ V. The cantilever tip makes contact with the CNT at the midpoint between source and drain only during tip gate measurement. Arrows represent the direction of the voltage sweep. (b) Force−distance curve (top) and corresponding current modulation (bottom) in the CNT at $V_{GS} = 0$ V and (c) at $V_{GS} = -15$ V. The cantilever is grounded ($V_{TS} = 0$ V) and makes contact with the CNT at midpoint. $V_{DS} = 2$ V for both cases. Black and red arrows in top vignettes show approaching and retracting curves, respectively. Negative gate voltages lead to higher tip pull-off (adhesion) force due to electrostatic interaction. In contrast, the sign and magnitude of current modulation in the CNT are strongly influenced by the back gate voltage.

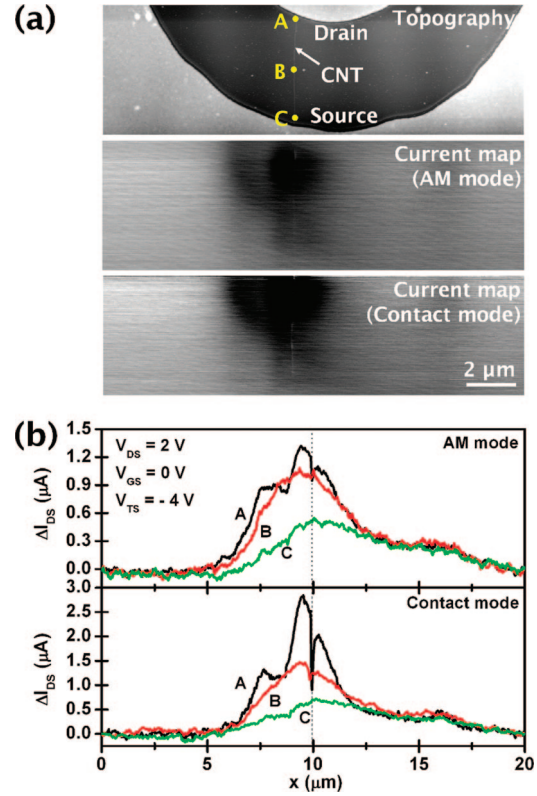

Figure 4. (a) AFM topography of the CNTFET from Figure 1c in AM mode and corresponding current modulation maps in the CNT at $V_{DS} = 2$ V, $V_{GS} = 0$ V, and $V_{TS} = -4$ V in AM and contact modes. Darker areas correspond to higher, and lighter areas correspond to lower current. (b) Cross-sectional plots of the current modulation (ΔI_{DS}) in the CNT at three positions: A is near the drain, B is at the midpoint between electrodes, and C is near the source. Current flow between the tip and CNT is negligibly small (<0.1 nA) compared to ΔI_{DS}.

First, current-gate voltage ($I_{DS}-V_{GS}$) transfer characteristics of the CNTFET were measured. Figure 3a shows $I_{DS}-V_{GS}$ curves using either the substrate back gate or AFM tip gate, when voltage is swept forward and backward (indicated by arrows) from −15 to 15 V at $V_{DS} = 0.05$ V. The cantilever was placed far away from the CNT when the device was back-gated and it was near the midpoint of the CNT when the device was tip-gated. The tested CNTFET exhibited p-type conduction with current flow significantly suppressed as the gate voltage increases. On/off current ratio was between 11500 and 17000 with the device back gated and between 1700 and 3000 while tip gated. Hysteresis existed for both cases, attributed to the presence of water-silanol surface traps,[26] as well as charge trapping in the oxide layer.[27−29] While the planar back gate had global control over device power switching, the tip gate offered local control. The gates could be used separately or together.

Instead of making contact with the CNT during $I-V$ measurements, the cantilever tip approached or withdrew from the midpoint between the two electrodes to examine capacitive coupling and effect of contact on current modulation as a function of nanotube-tip distance. Figure 3b,c shows such force−distance curves (top vignette) and corresponding current modulation (bottom vignette) in the CNTFET with the back gate at 0 and −15 V, respectively. The cantilever tip was grounded ($V_{TS} = 0$ V) and the drain held at $V_{DS} = 2$ V for both cases. Similar force−distance curves were observed for both ground and negative back gate voltage, while the cantilever bent further downward during engagement and experienced higher pull-off (adhesion) force due to electrostatic interaction with negative gate bias. When the back gate was grounded, current flow increased as the cantilever approached the CNT. However, when the back gate was negatively biased, current flow decreased as the cantilever approached the CNT. Current modulation became negligible after the cantilever tip made contact with the CNT

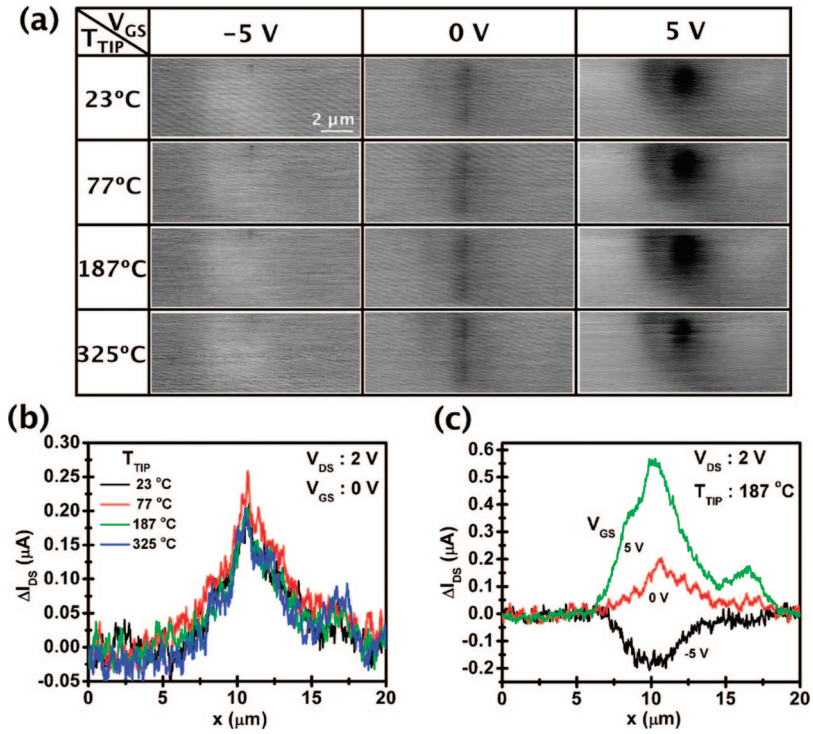

Figure 5. (a) Current modulation maps at various tip temperatures and back gate voltages in AM mode. (b) Cross-sectional plots of the current modulation in the CNT across the midpoint between the drain and source at $V_{DS} = 2$ V and $V_{GS} = 0$ V while the cantilever tip temperature (T_{Tip}) varies from 23 to 325 °C. (c) Cross-sectional plots of the current modulation in the CNT across the midpoint between the drain and source at $V_{DS} = 2$ V and $T_{Tip} = 187$ °C while V_{GS} varies from −5 to 5 V.

for both cases. More noticeable change in current modulation was observed with negative gate bias. Overall, the sign and magnitude of current modulation in the CNTFET were strongly influenced by the back gate voltage and physical contact might not play a role. Point-by-point force−distance measurement is somewhat time-consuming, so it is recommended to measure current modulation while the cantilever tip scans over the entire CNTFET.

Figure 4a shows AFM topography of the CNTFET using AM mode and corresponding current modulation maps in the CNTFET in AM and contact modes with voltage biases as stated in Figure 4b. The CNTFET imaged was the same as the one previously shown in Figure 1c and imaging conditions were also identical to those previously described. Both current maps had the same data range for comparison. In general, current flow in the CNTFET increased when the negatively biased cantilever tip was held nearby (dark and bright areas indicate current increase and decrease, respectively). However, when the biased tip was placed right over the CNT, current flow was locally suppressed. These general observations were more pronounced in contact mode than in AM mode since contact mode offered stronger capacitive coupling due to the reduced gap between the tip and CNT, and maintained contact during entire imaging.

To quantitatively compare the two imaging modes, cross-sectional plots of the current modulation in the CNTFET across three points were made and shown in Figure 4b. The current modulation was more significant when the negatively biased tip was close to the drain (location A). Contact effects were also significant near the drain. Each contact point became a scattering center thus decreasing the current in the CNT. Although strong current modulation could be observed in contact mode, it is recommended to use AM mode to minimize tip wear especially when the tip is biased to generate high electric fields, or heated to high temperatures. Further studies were carried out on the effect of tip-gate vs back-gate on the current modulation of the CNTFET, as described in the Supporting Information.

Unique to our study, the CNTFET could also be locally heated, to investigate the local temperature effect of a heated AFM tip in AM mode with and without biasing the back gate. Local heating could affect the electrical transport of a CNT by increasing the scattering rate, and local heating may also be able to modify the Fermi level toward the conduction band by locally desorbing oxygen molecules.[30] Figure 5a shows current modulation maps in the CNTFET when the cantilever tip temperature varies between 23 and 325 °C and the back gate varies between −5 and 5 V. These were obtained while imaging the same CNTFET shown in Figure 4a. Figure 5b shows cross-sectional plots of the current modulation in the CNTFET across the midpoint between electrodes at $V_{DS} = 2$ V and $V_{GS} = 0$ V while the cantilever tip temperature (T_{Tip}) varies from 23 to 325 °C, and Figure 5c shows cross-sectional plots of the current modulation across the midpoint at $V_{DS} = 2$ V and $T_{Tip} = 187$ °C while V_{GS} varies from −5 to 5 V. In contrast to experiments with local electric fields (see Supporting Information, Figure S3), we find local heating up to 325 °C had only a small effect on the current modulation, although the current does decrease slightly at higher tip temperature. Overall, the current

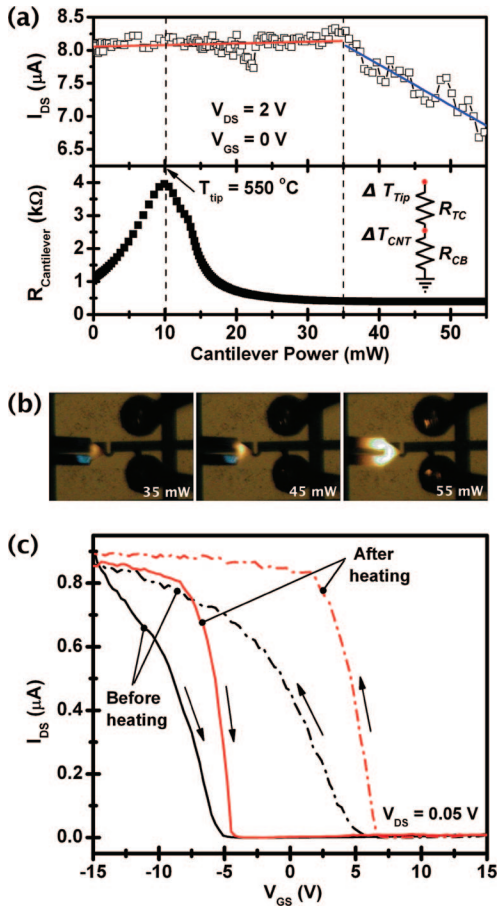

Figure 6. (a) Current flow (I_{DS}) in the CNTFET as a function of the cantilever power while the cantilever tip makes contact with the CNT at the midpoint between source and drain. The corresponding cantilever resistance is similarly shown as a function of the cantilever power. While the cantilever power is swept, its tip maintains contact with the CNT with a constant deflection set point. The inset shows an equivalent thermal circuit including tip-tube and tube-substrate resistances. (b) Optical images of the setup at cantilever power of 35, 45, and 55 mW, showing the glowing hot tip. (c) $I_{DS}-V_{GS}$ curves of the CNTFET with the planar back gate at $V_{DS} = 0.05$ V and $V_{TS} = 0$ V before and after high temperature tip heating at the midpoint between source and drain. Arrows represent the direction of the gate voltage sweep.

modulation maps at different tip temperatures looked similar to the ones with the tip grounded at room temperature since each leg was symmetrically biased to maintain ground at the tip ($V_{TS} = 0$).

Higher temperature experiments were performed with the cantilever tip heated above 1000 °C. Instead of scanning over the CNT, the heated tip was stationary and maintained contact with the CNT approximately at its halfway point to ensure better thermal conductance. The contact force was kept below 12 nN using the feedback control in the AFM (initially, the contact force was fixed at 12 nN at room temperature, but decreased as the cantilever was heated and became softer). While the cantilever power was increased stepwise far beyond its thermal runaway point in conjunction with a current limiting resistor,[17] current flow in the CNTFET was measured as shown in Figure 6a. The CNT current was almost insensitive to local heating from the cantilever when the cantilever power was <35 mW, but the current started to decrease linearly with cantilever power >35 mW. Figure 6b shows optical images when the cantilever power was 35, 45, and 55 mW, respectively. Each shows the cantilever glowing and emitting light from its free end and this glowing area and intensity of light increase with the cantilever power. Corresponding temperatures were estimated[31,32] to be 865, 990, and 1170 °C, respectively. The current modulation of the CNT was approximately −0.7 μA when the tip was near 1000 °C.

To estimate the temperature rise in the CNT, both self-heating for the given operating conditions and temperature-dependent electrical conductance were considered. Averaged temperature rise due to self-heating at $V_{DS} = 2$ V and $I_{DS} = 8$ μA was estimated to be less than 10 °C for a 2 nm diameter and 4 μm long single-wall CNT.[33] This was the baseline for additional tip heating that can be deduced from the electrical conductance modulation of the CNT under the tip-induced temperature increase, $dG/dT \approx -12.5$ nS/K at the applied $V_{DS} = 2$ V for a nanotube of this length. We note this is the intrinsic conductance modulation of the CNT, which has an additional contact series resistance of approximately $R_C \approx 180$ kΩ. These values are derived from a comparison between our simulations[33] and the present experimental data and also similar to recent results reported elsewhere.[16] Thus, in order to observe the approximately monotonous current decrease beyond 35 mW cantilever power, an average CNT temperature increase $\Delta T_{CNT} \approx 81$ °Cabove the baseline is expected at 45 mW, and $\Delta T_{CNT} \approx 155$ °C is expected at 55 mW tip power. These values are far below the temperature at which CNTs break down by oxidation (~600 °C),[33] explaining the resilience of the nanotube despite the high cantilever temperatures. The thermal resistance between the heated tip and the CNT can be estimated from the simple thermal circuit in the Figure 6a inset, or $R_{TC} = R_{CB}(\Delta T_{Tip}/\Delta T_{CNT} - 1)$. Here $R_{CB} = 1/(gL) \approx 1.5 \times 10^6$ K/W is the thermal resistance between CNT and the substrate or "back",[34] where g is the thermal conductance per unit length and L is the length of the CNT. The thermal resistance between the heated tip and nanotube was therefore estimated at $R_{TC} \approx 1.6 \times 10^7$ K/W at 45 mW cantilever power, and 9.6×10^6 K/W at 55 mW cantilever power. This resistance is of comparable magnitude to that between a heated tip and a metal nanothermometer.[32] The tip-nanotube thermal resistance decreases at higher heater power and temperature, as temperature-dependent heat transfer mechanisms such as radiation increase in strength. In addition, it is interesting to note that below 35 mW heater power, the CNT current is essentially unchanged. This signifies a much higher tip-nanotube thermal resistance at lower temperatures, the result of water and organic layers covering the nanotube and SiO_2 surface, which dissipate as the temperature increases.

To quantify the final observation, the CNT was electrically measured again to examine any changes after the tip-induced heating. As shown in Figure 6c, the $I_{DS}-V_{GS}$ transfer characteristics were somewhat changed after the high temperature heating experiments. The general trends including the hysteresis were similar. However, the transconductance ($|dI_{DS}/dV_{GS}|$) was improved, confirming an "annealed" surface

and improved nanotube mobility. A higher temperature range in a controlled atmosphere (either inert gas or vacuum) at various contact forces may be explored in the near future, although care must be taken to avoid irreversible damage to the nanotube or the cantilever.

In summary, we have investigated the current modulation of a single-wall carbon nanotube field-effect transistor using an AFM cantilever that is capable of applying local electric and temperature fields in both contact and amplitude modulation modes. From force−distance measurements and contact mode imaging, we found out the sign and magnitude of current modulation in the CNTFET were strongly influenced by the back gate voltage, and contact effect on the current modulation was asymmetric and very strong near the drain electrode. Then, local electric field and local heating effects on the current modulation of the CNTFET were examined. Whereas significant current modulation was observed with the local electric field, local heating effect on the current modulation was negligible up to 325 °C tip temperature in air. To further investigate the tip-nanotube thermal coupling, the cantilever tip was heated to near 1000 °C elevating the average nanotube temperature by up to 155 °C, and a heated tip-nanotube thermal resistance of approximately 1.6×10^7 K/W was obtained. Our results showed general characteristics of a conductive and heated AFM cantilever tip as a moving gate over nanotube field-effect devices that enable novel electrothermal current microscopy on nanoelectronic devices.

Acknowledgment. This work was supported by DARPA including a DARPA Young Faculty Award for EP, and by the Nanoelectronics Research Initiative (NRI) through the Midwest Institute for Nanoelectronics Discovery (MIND).

Supporting Information Available: Additional experimental details on CNT cutting, surface potential mapping, and back-gate versus tip-gate modulation. This material is available free of charge via the Internet at http://pubs.acs.org.

References

(1) Tans, S. J.; Verschueren, A. R. M.; Dekker, C. *Nature* **1998**, *393* (6680), 49–52.
(2) Derycke, V.; Martel, R.; Appenzeller, J.; Avouris, P. *Nano Lett.* **2001**, *1* (9), 453–456.
(3) Treacy, M. M. J.; Ebbesen, T. W.; Gibson, J. M. *Nature* **1996**, *381* (6584), 678–680.
(4) Pop, E.; Mann, D.; Wang, Q.; Goodson, K.; Dai, H. J. *Nano Lett.* **2006**, *6* (1), 96–100.
(5) Tombler, T. W.; Zhou, C. W.; Alexseyev, L.; Kong, J.; Dai, H. J.; Lei, L.; Jayanthi, C. S.; Tang, M. J.; Wu, S. Y. *Nature* **2000**, *405* (6788), 769–772.
(6) Minot, E. D.; Yaish, Y.; Sazonova, V.; Park, J. Y.; Brink, M.; McEuen, P. L. *Phys. Rev. Lett.* **2003**, *90* (15), 156401.
(7) Tans, S. J.; Dekker, C. *Nature* **2000**, *404* (6780), 834–835.
(8) Freitag, M.; Johnson, A. T.; Kalinin, S. V.; Bonnell, D. A. *Phys. Rev. Lett.* **2002**, *89* (21), 216801.
(9) Kalinin, S. V.; Bonnell, D. A.; Freitag, M.; Johnson, A. T. *Appl. Phys. Lett.* **2002**, *81* (27), 5219–5221.
(10) Zhou, X.; Dayeh, S. A.; Wang, D.; Yu, E. T. *Appl. Phys. Lett.* **2007**, *90* (23), 233118.
(11) Koley, G.; Lakshmanan, L.; Wu, H.; Cha, H. Y. *Phys. Status Solidi A* **2007**, *204* (4), 1123–1129.
(12) Zhang, L. M.; Fogler, M. M. *Nano Lett.* **2006**, *6* (10), 2206–2210.
(13) Hackens, B.; Martins, F.; Ouisse, T.; Sellier, H.; Bollaert, S.; Wallart, X.; Cappy, A.; Chevrier, J.; Bayot, V.; Huant, S. *Nat. Phys.* **2006**, *2* (12), 826–830.
(14) Topinka, M. A.; LeRoy, B. J.; Shaw, S. E. J.; Heller, E. J.; Westervelt, R. M.; Maranowski, K. D.; Cossard, A. C. *Science* **2000**, *289* (5488), 2323–2326.
(15) Jura, M. P.; Topinka, M. A.; Urban, L.; Yazdani, A.; Shtrikman, H.; Pfeiffer, L. N.; West, K. W.; Goldhaber-Gordon, D. *Nat. Phys.* **2007**, *3* (12), 841–845.
(16) Tsen, A. W.; Donev, L. A. K.; Kurt, H.; Herman, L. H.; Park, J. *Nat. Nanotechnol.* **2009**, *4*, 108–113.
(17) Lee, J.; Beechem, T.; Wright, T. L.; Nelson, B. A.; Graham, S.; King, W. P. *J. Microelectromech. Syst.* **2006**, *15* (6), 1644–1655.
(18) Szoszkiewicz, R.; Okada, T.; Jones, S. C.; Li, T. D.; King, W. P.; Marder, S. R.; Riedo, E. *Nano Lett.* **2007**, *7* (4), 1064–1069.
(19) Gotsmann, B.; Duerig, U.; Frommer, J.; Hawker, C. J. *Adv. Funct. Mater.* **2006**, *16* (11), 1499–1505.
(20) King, W. P.; Saxena, S.; Nelson, B. A.; Weeks, B. L.; Pitchimani, R. *Nano Lett.* **2006**, *6* (9), 2145–2149.
(21) Nelson, B. A.; King, W. P. *Rev. Sci. Instrum.* **2007**, *78* (2), 023702.
(22) Remmert, J. L.; Wu, Y.; Lee, J. C.; Shannon, M. A.; King, W. P. *Appl. Phys. Lett.* **2007**, *91* (14), 143111.
(23) Liao, A.; Zhao, Y.; Pop, E. *Phys. Rev. Lett.* **2008**, *101*, 256804.
(24) Collins, P. C.; Arnold, M. S.; Avouris, P. *Science* **2001**, *292* (5517), 706–709.
(25) Park, J. Y.; Yaish, Y.; Brink, M.; Rosenblatt, S.; McEuen, P. L. *Appl. Phys. Lett.* **2002**, *80* (23), 4446–4448.
(26) Kim, W.; Javey, A.; Vermesh, O.; Wang, O.; Li, Y. M.; Dai, H. J. *Nano Lett.* **2003**, *3* (2), 193–198.
(27) Fuhrer, M. S.; Kim, B. M.; Drkop, T.; Brintlinger, T. *Nano Lett.* **2002**, *2* (7), 755–759.
(28) Radosavljevi, M.; Freitag, M.; Thadani, K. V.; Johnson, A. T. *Nano Lett.* **2002**, *2* (7), 761–764.
(29) Vijayaraghavan, A.; Kar, S.; Soldano, C.; Talapatra, S.; Nalamasu, O.; Ajayan, P. M. *Appl. Phys. Lett.* **2006**, *89* (16), 162108.
(30) Kamimura, T.; Matsumoto, K. *Jpn. J. Appl. Phys., Part 1* **2005**, *44* (4A), 1603–1605.
(31) Lee, J.; Wright, T. L.; Abel, M. R.; Sunden, E. O.; Marchenkov, A.; Graham, S.; King, W. P. *J. Appl. Phys.* **2007**, *101* (1), 014906.
(32) Park, K.; Cross, G. L. W.; Zhang, Z. M.; King, W. P. *J. Heat Transfer* **2008**, *130*, 102401.
(33) Pop, E.; Mann, D.; Goodson, K.; Dai, H. *J. Appl. Phys.* **2007**, *101*, 093710.
(34) Pop, E. *Nanotechnology* **2008**, *19*, 295202.

NL803024P